Meas. Sci. Technol. **19** (2008) 055301 (8pp) doi:10.1088/0957-0233/19/5/055301

Parallel detection of low modulation depth signals: application to picosecond ultrasonics

R J Smith[1], M G Somekh[1], S D Sharples[1], M C Pitter[1], I Harrison[1] and C Rossignol[2]

[1] School of Electrical and Electronic Engineering, University of Nottingham, University Park, Nottingham, NG7 2RD, UK
[2] Laboratoire de Mécanique Physique, UMR CNRS 5469, Université Bordeaux 1, 351 cours de la Libération, 33405 Talence, France

Received 20 November 2007, in final form 15 February 2008
Published 19 March 2008
Online at stacks.iop.org/MST/19/055301

Abstract
We demonstrate parallel detection of laser ultrasonic signals above 50 GHz, where the signals are encoded as small modulations on a large dc background signal. The measurement problem addressed here is generic for many situations, particularly pump/probe experiments, and this paper discusses the problems of moving from single point to parallel detection and practical solutions. This is achieved with a commercial detector array, custom interface electronics and a carefully selected phase stepping algorithm. The parallel detection of Brillouin oscillations illustrates the very low modulation depths that can be measured with this technique. Noise performance and projected improvements for future custom detectors are also considered.

Keywords: arrays, demodulation, optical sensors, ultrasonic measurement

(Some figures in this article are in colour only in the electronic version)

1. Introduction

One recurring measurement problem in optical measurement is the need to recover weakly modulated signals in a large background. For instance, this occurs in nearly all pump/probe experiments where a small proportion of the modulation imposed on the pump beam is transferred to the probe beam. Examples include: photoreflectance [1], photothermal techniques [2] and laser ultrasonics [3]. These pump/probe techniques are usually performed as point measurements; an exciting and important challenge is to perform many such pump/probe measurements in parallel. This would greatly speed up measurements that are often time consuming, and will furthermore enable measurements to be made that are presently impractical. In this paper we show how modulated signals can be detected in parallel with comparable performance to point detection with a photodiode/lock-in amplifier combination. The method employed here uses a commercial array detector, some custom interface electronics and a suitable phase stepping algorithm to suppress the odd harmonics inherent to square wave modulation. In addition, we discuss future full custom designs that will surpass the performance of the array described in the present paper.

The typical point detection approach is usually implemented with a modulator, a photodetector and a lock-in amplifier. Here, the signal of interest is mixed with a reference signal and integrated or band pass filtered to allow narrow-band detection. In the case of optical signals a mechanical chopper or acousto-optical modulator is often used to impose the reference frequency on the optical signal. The signal from the photodiode is used as the input to the lock-in amplifier and the signal driving the chopper or modulator is used as the frequency reference and this produces an extremely sensitive detection system [4].

Many experimental situations benefit from parallel detection schemes. This has been successfully achieved by integrating the signal over parts of the cycle and recovering the signal with a phase stepping algorithm. For instance, in thermography, where the temperature changes induced by a sinusoidally modulated heat source are recorded, parallel detection [5] is quite common. The method has also been applied to parallel heterodyne interferometry [6]. The

 © 2008 IOP Publishing Ltd Printed in the UK

concept behind the approach used in previous work forms the basis of the technique applied in this paper; however, the method used here copes with non-sinusoidal modulation and, more significantly, recovers signals with modulation depths orders of magnitude smaller than those detected in previous experiments.

In our case we require parallel detection to speed up the experiment time and reduce the impact of environmental drift. In our experiments, in which Brillouin oscillations are generated [7], the modulation signal of interest is typically 10^4–10^5 times smaller than the dc light level. The principle behind Brillouin oscillations is discussed in more detail in section 3, but briefly, they arise from extremely high-frequency laser ultrasound which is detected as a variation on the background reflection. The Brillouin oscillations relate the longitudinal sound velocity to the refractive index of the material and can also be used to observe small subsurface discontinuities in the sample. The results presented here represent the first report of parallel detection of several hundred channels of laser generated GHz ultrasound; in this paper we will describe the detection issues necessary to achieve these measurements and argue that the solution is applicable to many other measurement situations.

Small signals and parallel detection impose certain common requirements on the detection system to be used; these requirements are:

- The approach should be scaleable up to a large number of channels with realistic demands on the analogue-to-digital converter (ADC) employed.
- The system needs to be able to detect many photons so that the required SNR and dynamic range are obtained.
- Coherent noise should be sufficiently well suppressed that signal averaging improves the SNR to the required level.

In addition the following are often important:

- The technique measures both the amplitude and phase of the signal of interest.
- The system needs to cope adequately with square wave modulation, by which we mean that the amplitude/phase cross-talk with non-sinusoidal modulation needs to be controllable. This is particularly important in the experiments we describe here.

2. Parallel detection of low level modulation

We will divide this section into two parts describing some general considerations and specific issues that arose with our own implementation.

2.1. General considerations

To detect small signals with point detectors the usual approach is to use lock-in detection as discussed in section 1. An alternative method is to use phase stepping techniques [8] where the signal is sampled at different parts of its cycle and recovered with a suitable algorithm. It is possible to perform parallel detection with either of these approaches. Parallel lock-in detection with multiple lock-in amplifiers has been implemented using custom silicon integrated circuits both by our group and others [9–11]. Useful performance can be achieved with this approach, the problem, however, is that the limited area of silicon and electrical power available, furthermore the restricted library of components mean that it is not practical to get performance that challenges single point lock-in detection. An earlier work [10] used a 'smart detector array' for a spectrally resolved measurement of carrier dynamics in a thin sample of bulk GaAs. This detector was custom built by the authors and is not available commercially. It consisted of an array of miniature envelope detectors integrated into a single chip. Each channel of the device consisted of a photodiode and load, an amplifier, a band pass filter, a rectifier and a low pass filter to integrate [12].

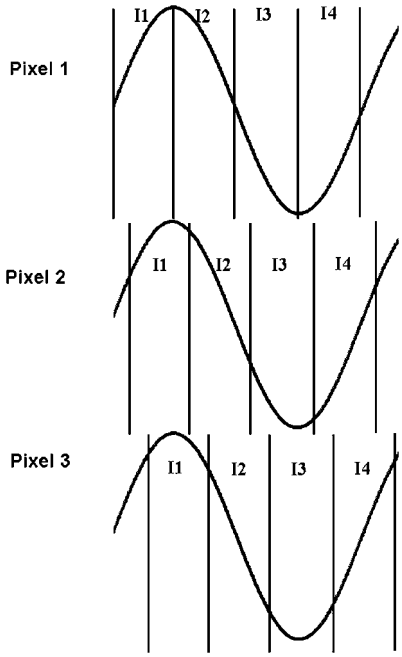

Figure 1. Diagram explaining the principle of the lock-in detection for the case where four phase steps are used. The effect of the rolling shutter is demonstrated for each pixel where phase of data acquisition varies across the array.

The approach described here is quite different. Rather than using custom built continuous time circuitry, we employ an integrating detector and use phase stepping to demodulate the signal. Moreover, we measure modulation depths between one and two orders of magnitude smaller than those of Bourquin *et al* [10]. The concept behind integrated detection is shown in the upper trace of figure 1. For pixel 1 the integration for I1 starts at $t = 0$; the detector continues to integrate the sample until the signal is ready to be read out. Similarly, I2, I3, I4 etc are obtained by integrating over similar time intervals; a suitable algorithm is then used to recover the amplitude and/or phase of the output signal. In addition to the modulated part of the signal shown in figure 1, there is also a (very) large constant background; this generates noise that tends to swamp the modulation. Even if the only noise source is shot noise there is a requirement to detect large number of photons, for instance, to recover a modulation depth of 10^{-6} implies that

at least 10^{12} photons need to be detected. This places a severe constraint on integrating optical detectors since it places a requirement on having a very large well capacity or the ability to read out the data very rapidly which, in turn, increases the read-out noise.

Ideally, one would want to read all the pixels out simultaneously since the reference phase will be constant for each pixel. In practice, commercial sensors tend to use a rolling, rather than a global shutter, so that each pixel in the array can be exposed and read out in series. This avoids the need for sample and hold circuitry while enabling a single output amplifier to be used for the whole array, allowing a simple (and cost-effective) design. The effect of this is shown in figure 1 which shows how the read-out time of each pixel changes. For an array with 512 pixels (as used in this study) the integration time per pixel is constant; however, due to the rolling shutter the phase recorded by each pixel changes across the array. The rolling shutter approach requires that the pixels are read out sequentially so that one channel on the ADC captures all of the data.

To recover the modulated signal integrated signals from each pixel are acquired and recovered using a phase stepping algorithm. In principle for sinusoidal modulation only three phase steps are necessary although it is more usual to use four phase steps produced by integrating over one fourth of the modulation cycle. It is easy to generalize the phase stepping algorithms to N equal steps as described below:

$$\Delta\alpha = \frac{2\pi}{N} \tag{1}$$

$$S_1 = \sum_{m=0}^{N-1} I_m \cos\alpha_m \tag{2}$$

$$S_2 = \sum_{m=0}^{N-1} I_m \sin\alpha_m \tag{3}$$

$$\text{Amplitude} = \sqrt{S_1^2 + S_2^2} \tag{4}$$

$$\text{Phase} = \tan^{-1}\left(\frac{S_2}{S_1}\right) \tag{5}$$

where $\Delta\alpha$= phase step increment, I_m = measured signal for step m, α_m = phase step angle for the mth step.

We now discuss the implications of the number of phase steps on the results presented here. Firstly, we consider the effect of signal-to-noise ratio assuming ideal shot noise limitation. Provided a constant number of photons are detected for each modulation cycle the noise level will remain the same regardless of how many steps are used. The recovered signal, however, will be larger if more steps are used. It can be shown (see the appendix) that for sinusoidal modulation (or the fundamental component of non-sinusoidal modulation, which applied in our case) the recovered ac signal amplitude is proportional to $\frac{N}{\pi}\sin\left(\frac{\pi}{N}\right)$. For the three-step method the recovered signal amplitude for a modulation of one unit is 0.83 whereas for the seven-step method it is 0.96; this is 15.6% larger, and because of this the signal-to-noise ratio will improve slightly with increasing numbers of phase steps.

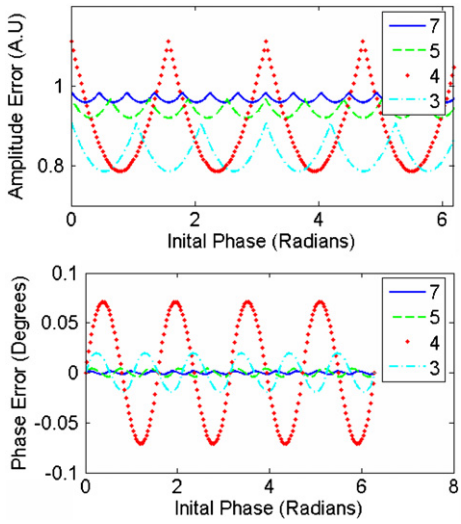

Figure 2. Diagram showing amplitude phase cross-talk for square wave modulation. The figure shows the recovered amplitude (top) and phase (bottom) versus signal phase when algorithms corresponding to equations (1) to (5) are used. The legend shows the variation for algorithms employing different numbers of phase steps.

In our experiments and many others a chopper is used, which means that the modulation waveform is non-sinusoidal; indeed the actual waveform approaches a square waveform when the optical beam is narrow compared to the aperture of the chopper. For square wave modulation, or any modulation waveform with significant odd harmonics, a serious problem with the phase stepping approach arises particularly when a rolling shutter is used. In this case the apparent phase of signals will vary with pixel position as shown in figure 1. The algorithms described by equations (1)–(5) are sensitive to the presence of odd harmonics of the modulation frequency. For square wave modulation these odd harmonics have a dramatic effect, since they introduce large systematic errors in the recovered amplitude and phase. Figure 2 shows the amplitude and phase recovered for a square wave signal for algorithms with different numbers of phase steps as a function of the initial phase of the square wave. The errors are periodic, with the period related to the number of steps used in the algorithm. When the number of phase steps is odd the error oscillates through $2N$ cycles per modulation cycle.

The peak-to-peak variation of these amplitude errors is shown in table 1. It is apparent that these errors decrease with the number of phase steps, with errors decreasing monotonically for both even and odd numbers of phase steps. As the number of phase steps increases, the algorithm approaches a continuous time measurement where only the fundamental frequency is detected. The errors on the curve for odd numbers of phase steps are far smaller than those for even numbers. Even stepped algorithms are insensitive to even harmonics but particularly prone to errors when square modulation is used.

In our experiment these errors correspond to the fluctuations in the amplitude that arise from using one of the algorithms described in equations (1)–(5) without

Table 1. Systematic errors introduced to recovered amplitude and phase by square wave modulation.

Steps	Error in amplitude (per cent)	Maximum phase error (deg)
3	12.15	2.234
4	32.53	8.15
5	4.73	0.465
6	14.03	2.234
7	2.46	0.168
8	7.81	0.919
11	1.01	0.0430
15	0.546	0.0169
25	0.197	0.0036

compensating for the variations in phase caused by the moving shutter. It is highly inconvenient to introduce this extra complexity, especially as the precise modulation may deviate from a square wave, therefore, it is desirable to use a number of phase steps that ensures that the amplitude phase cross-talk is kept to an acceptable level.

In the work described here, we were concerned with amplitude/phase cross-talk and not the phase itself, however, in many experiments the phase is an important measurand and the third column of table 1 quantifies the maximum phase error when perfect square wave modulation is used. The trends are essentially similar to those for the amplitude error decreasing with increasing numbers of phase steps and giving smaller errors for odd numbers of phase steps.

In summary, larger numbers of phase steps reduce the amplitude/phase cross-talk and also increase the amplitude of the signal recovered at the fundamental frequency. The additional complexity and reduction in overall modulation frequency means that an appropriate compromise has to be made in the determination of the optimum number of phase steps; this is discussed for our specific case in the following subsection.

2.2. *Specific implementation*

The most important single consideration is to choose an optical detector that gives sufficient signal-to-noise ratio. For this reason we chose to use a linear array of 512 pixels (Hamamatsu S3924-512Q,F). Each pixel has a saturation charge of 50 pC which allows up to 3.12×10^8 photons to be stored. This large well depth gives us the potential for detection of very small modulations. The maximum read-out speed per pixel is 500 kHz: this gives a theoretical maximum frame rate of $5 \times 10^5/512$ Hz, although in practice a small amount of dead time, equivalent to the time required to read four pixels, must be included at the end of each frame read-out to permit a master reset of the array. The actual frame rate is therefore $5 \times 10^5/516$ Hz, or 969 Hz.

The detector parameters above set the conditions for the rest of the electronic detection. The number of detectable photons sets an optimum voltage signal to noise ratio of approximately 18 000; this implies the use of an ADC with at least 15 bits. The 500 kHz pixel rate sets the minimum sampling rate for the ADC. For this reason the ADC we used was a NI-6281 which has a depth of 18 bits and a 625 k samples s^{-1} sample rate in single channel operation.

In view of the maximum frame rate of 969 Hz there is a compromise between the modulation frequency induced by the chopper speed and the number of phase steps used in the algorithm. As the number of steps increases the chopper frequency decreases (chopper frequency is $969/N$ Hz) and this means that although the systematic errors decrease. At some point the random noise will get worse from working in a noisier part of the spectrum, close to baseband. A good compromise in our case was to use seven phase steps. In our case where the signal-to-noise ratio of the final signal is relatively small because we wish to extract very low modulation depths these errors are not problematic. In practice the finite width of the beam that passes through the chopper means the modulation is not quite square; this reduces the odd harmonics, so the actual error is less than the 2.55% quoted in table 1.

In order for the phase stepping algorithm to work correctly, the mechanical chopper that modulates the light must be synchronized with the array detector read-out, such that an integer number of readings for each and every pixel are acquired for every chopper cycle. If we term the sequential reading of all the pixels in the array a 'frame', then the simplest way that this can be achieved is by dividing a clock signal that occurs once every frame by the number of steps desired in the phase stepping algorithm. This new, divided-down clock is then used to synchronize the mechanical chopper. To facilitate the implementation of this chopper synchronization clock, a custom pulse generator board was designed and implemented for the detector array.

To summarize: we have chosen an array detector to provide the required well depth and signal to noise ratio and selected an ADC with sufficient bit depth and data acquisition speed. A suitable algorithm was then chosen to give a good compromise for amplitude/phase cross-talk and modulation frequency. Finally synchronization electronics were produced that locked the clock of the detector array to the chopper modulation frequency.

Unfortunately, there was one more issue that needed addressing before satisfactory performance could be assured; this arose because of the nature of the signals emerging from the detector array. The data stream output from the array shares some of the characteristics of a video data stream, and is illustrated in figure 3(*a*), which is a trace of the data signal captured for several pixels. We note that the duty cycle of the signal is low; the data are guaranteed to be at the correct voltage level for only one sixth of a cycle. For the rest of the time the level is either at or around 0 V, or rising from this low voltage to the correct level. There are sharp transitions between the two regions. This profile of the data signal imposes severe requirements on the ADC used to acquire the data, as it is not simply sufficient for the ADC to have a sample rate that matches the data rate. The solution is to either use an ADC with significantly higher capabilities or to alter the data signal to increase the duty cycle. This can be achieved with a track and hold circuit, which alters the signal such that the one shown in figure 3(*b*) is instead presented to the ADC. The performance requirements of the ADC are then significantly reduced.

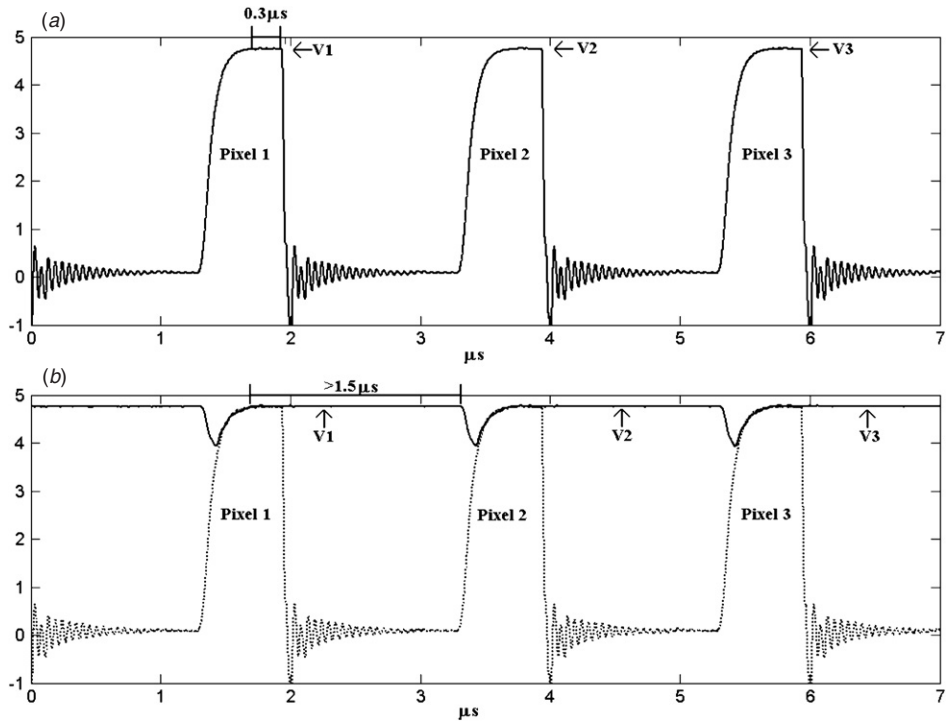

Figure 3. Schematic diagram showing use of track and hold circuit. (*a*) Streamed signal output from the detector array, showing output from several pixels, (*b*) the same output after passing through track and hold circuit, to reduce the demands on the analogue-to-digital converter.

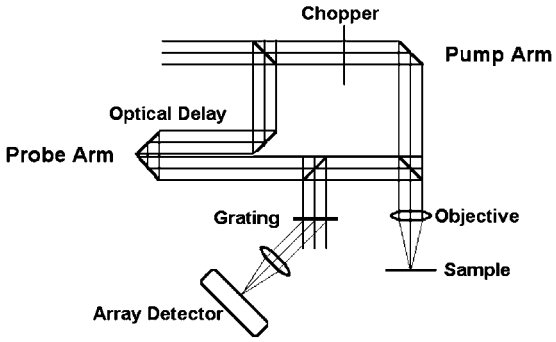

Figure 4. Schematic system diagram of optical configuration of the Brillouin oscillation experiment. The femtosecond laser source is not shown.

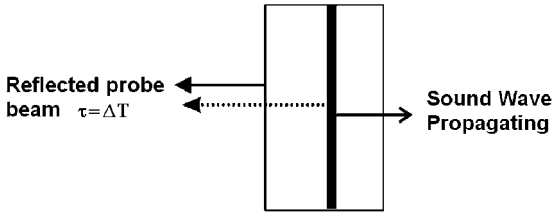

Figure 5. Diagram showing the origin of the Brillouin oscillation signal, essentially involving two beam interference between the surface of the sample and the travelling ultrasonic beam.

3. Example experimental results

The experimental system with which we used the detection system discussed in section 2 is shown in figure 4. This experiment employs a femtosecond laser (Spectra Physics Tsumani, 780 nm wavelength, 100 fs pulse width, 80 MHz repetition rate). The output of the laser is split into two arms for both pump and probe. The great majority of the power is directed into the pump beam (approx. 1 nJ per pulse); this is modulated by an optical chopper (whose frequency is controlled by the clock derived from the camera) and is focused onto the sample (see figure 4). The energy of the pump pulse is absorbed and causes rapid local heating and expansion of the sample. This induces a very high-frequency ultrasonic pulse in the sample. By changing an optical delay a pulsed probe beam (approximately 1000 times less intense than the pump) is used to measure the acoustic wave as it propagates into the sample. The detection process is explained in figure 5. The surface of the sample and the propagating longitudinal wave form an interferometer, where the phase between the interfering beams varies with the position of the sound wave. The delay between the probe and pump beams determines the position of the sound wave relative to the surface. Changing the delay between pump and probe enables the interference pattern to be recovered. The resulting patterns are termed Brillouin oscillations [5]. The frequency of these oscillations is given by $f_b = 2vn/\lambda$, where v is the acoustic velocity, n is the real part of the refractive index and λ is the wavelength of the probe beam in free space. For GaAs and a probe frequency of 780 nm the frequency of these oscillations is approximately 51 GHz. If either the sound velocity in the

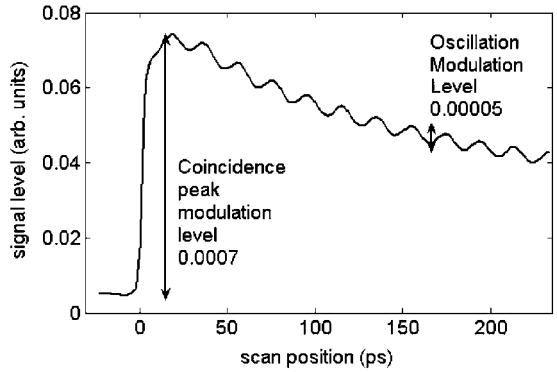

Figure 6. Brillouin oscillations recovered from the array at 780 nm wavelength. The coincidence peak signal level, $\Delta R/R$, is 0.0007 and the oscillation signal level is 0.00005.

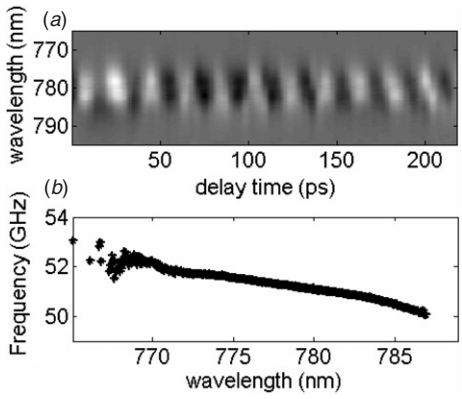

Figure 7. Ultrasonic results obtained with system. (*a*) Oscillations versus delay for different wavelengths. The grey scale represents the signal instantaneous signal level. (*b*) Plot of frequency versus wavelength from which sound velocity can be deduced.

solid or the refractive index is known the Brillouin oscillations allow the other parameter to be measured.

There is a considerable amount of information that may be extracted by measuring the Brillouin oscillations as a function of probe frequency. This has recently been carried out by [13] where a point detector was scanned at the output of a grating. In these experiments a very broadband probe was used, since the output from the pump laser was passed through a supercontinuum fibre. These measurements required scanning both the delay and the different wavelengths. Here, we show that the parallel detection scheme described above allows us to recover the whole spectrum simultaneously. The wavelengths to be measured were separated spatially by the use of a diffraction grating as shown in figure 4.

The output from the grating was focused onto the array so the wavelength varies across the array. Figure 6 shows the Brillouin oscillations obtained for one pixel of the array detector. At $t = 0$ the pump and probe beams are coincident in time and there is a relatively large change in signal due to thermal effects as the pump power is absorbed. Slow thermal relaxation of the sample then follow, and superimposed on this is the oscillatory signal corresponding to the propagation of sound waves. The coincidence peak is typically between

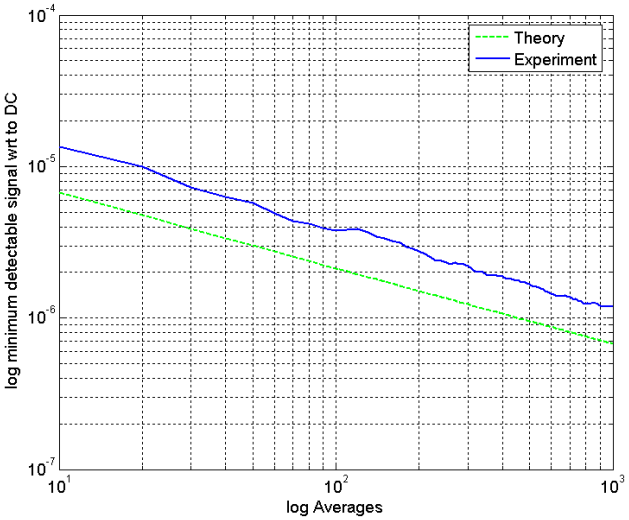

Figure 8. Noise signal measured versus signal averages. This shows the minimum detectable modulation after passing through phase stepping algorithm against number of signal averages (green curve), this is compared with the shot noise limit (blue curve).

10^3 and 10^4 times smaller than the dc light level (which is not shown). The oscillatory signal is approximately 10 times smaller than this (10^4 to 10^5 smaller than the dc level). Figure 7(*a*) shows the Brillouin oscillations as a function of wavelength (spread approximately ± 15 nm from 780 nm centre) and focused onto the linear array detector described previously when 400 averages were used. In these experiments the probe was simply the laser source; the use of a supercontinuum fibre would give a far greater spread of wavelengths and necessitate use of a coarser grating.

Figure 7(*b*) illustrates how the frequency of the oscillations changes with wavelength. These results closely agree with published values of velocity [14]; we can calculate the velocity for each wavelength using the measured frequency and the published values for the refractive index [14]. We obtain a mean velocity of 5383 m s^{-1} with a standard deviation of 3.4 m s^{-1} for the central 228 pixels. The value reported in [14] for the longitudinal velocity of GaAs along the [1 1 1] direction is 5390 m s^{-1}.

4. Noise performance

This detector has been used in combination with the seven step phase stepping algorithm to successfully recover modulation depths as low as 1.19×10^{-6}. In this case 1000 averages were acquired and the total measurement time was 7 s. The theoretical shot noise limit suggests that approximately 6.74×10^{-7} can be detected and so the actual detected signal is 1.76 times larger than the shot noise limit.

Figure 8 is a plot of the variation of the theoretical and detected modulation level as the number of averages is increased, both the curves decreasing with $\sqrt{N}$ for the range of measurements shown.

In order to examine the source of the excess noise the light source was blocked and the output measured and processed

according to the algorithm described earlier in section 2.1. In this case the rms output level was 5.05×10^{-6} V compared to 5.97×10^{-6} V at full illumination. The additional noise due to illumination is therefore (assuming they add incoherently) equal to $\sqrt{(5.97)^2 - (5.05)^2} \times 10^{-6} = 3.18 \times 10^{-6}$. This means that approximately 53% of the total noise power arises from readout noise. On this basis alone we would expect that the measured curve for minimum detected signal would be at least a factor of $\sqrt{\frac{100}{100-53}} = 1.46$ greater than the shot noise curve accounting for much of the difference from theory. The experimental results clearly confirm that small modulation depths can readily be recovered.

To obtain a scan with comparable SNR with the photodiode/lock-in combination takes approximately 25 s (4 averages at 6 s for each scan, plus a second to move to the next wavelength scan location). To obtain 512 scans would take approximately $3\frac{1}{2}$ h. The array took 22.5 min to acquire data in the 512 pixel array making the array 10 times faster than repeatedly scanning the single detector. The recorded data are also less susceptible to environmental changes between scans as all pixels are recorded together and are therefore all influenced by the same environmental factors. It must be emphasized that the greater speed of the parallel detection was achieved with tiny powers in the optical probe beam compared to those used with a point detector and lock-in amplifier. The maximum power that could be used with array was around 41 μW in total (80 nW per pixel), compared to up to 1 mW with a point detector. Indeed, it is the very small powers that the array can accept before saturation that is the main limitation of the present implementation of the system. A system that can utilize larger powers either with larger well capacity or faster read-out (without an associated increase in read-out noise) will give considerably faster data acquisition rates.

5. Discussion/conclusions

We have presented a technique for parallel detection of very weakly modulated signals. The approach we have taken is relatively insensitive to the influence of odd harmonics present in square wave modulation systems. The results presented show that results comparable to photodiode lock-in combination can be reproduced in a parallel form using the seven-step approach and a commercial detector array.

Our approach demonstrates that a commercially available sensor can be used for this application. However, we believe that there is still merit in fabricating a custom built array. We are currently designing a full-custom design that addresses some of the limitations of our present system. In contrast to [10] the design is based on integrating ('active') pixels, similar to the commercial design used for the results in this paper. Specifically, our custom design has a global shutter, a larger well capacity and higher read-out speed to boost the number of photons used and consequently reduce shot noise in the measurement. It also incorporates multiple sample and holds into each pixel to allow higher modulation frequencies to be used. Finally, it has random addressing, not possible in a rolling shutter design, which will allow us to allocate available bandwidth to pixels receiving the most light, while sampling less bright pixels less frequently.

Acknowledgment

The authors wish to acknowledge the financial support of the UK Engineering and Physical Science Research Council.

Appendix. Impact of varying the number of phase steps on recovered ac amplitude

For a phase stepping algorithm with N phase steps the effect of increasing the number of phase steps on the recovered ac amplitude can be derived. Consider the following:

$$i = 1 + a\cos(\phi + \phi_0) \tag{A.1}$$

where ϕ is the moving phase going between 0 and 2π and ϕ_o is the phase of the signal. Consider a series of phase steps with equal separation $\Delta\alpha$, starting at 0, $\Delta\alpha$, $2\Delta\alpha$, $3\Delta\alpha$ etc up to $2\pi - \Delta\alpha$: therefore $\Delta\alpha = \frac{2\pi}{N}$.

The ith signal is therefore

$$\begin{aligned} I_m &= \int_{\alpha_m}^{\alpha_m+\Delta\alpha} i(\phi)\,\mathrm{d}\phi \\ &= \int_{\alpha_m}^{\alpha_m+\Delta\alpha} 1 + a\cos\phi_0\cos\phi - a\sin\phi_0\sin\phi\,\mathrm{d}\phi \\ &= \Delta\alpha + a\cos\phi_0(\sin(\alpha_m+\Delta\alpha) - \sin(\alpha_m)) \\ &\quad + a\sin\phi_0(\cos(\alpha_m+\Delta\alpha) - \cos(\alpha_m)). \end{aligned} \tag{A.2}$$

This leads to a general expression for I_m,

$$\begin{aligned} I_m &= \Delta\alpha + 2a\cos\phi_0\cos\left(\alpha_m + \frac{\Delta\alpha}{2}\right)\sin\left(\frac{\Delta\alpha}{2}\right) \\ &\quad - 2a\sin\phi_0\sin\left(\alpha_m + \frac{\Delta\alpha}{2}\right)\sin\left(\frac{\Delta\alpha}{2}\right). \end{aligned} \tag{A.3}$$

The modulation, a, is obtained from

$$\mathrm{ac} = \sqrt{S_1^2 + S_2^2} \tag{A.4}$$

where

$$S_1 = \sum_{m=0}^{N-1} I_m \cos\alpha_m \tag{A.5}$$

$$S_2 = \sum_{m=0}^{N-1} I_m \sin\alpha_m. \tag{A.6}$$

The terms in $\cos\alpha_m$ and $\sin\alpha_m$ sum to zero, whereas the $\cos^2\alpha_m$ and $\sin^2\alpha_m$ apply a factor of $N/2$. This gives

$$\begin{aligned} S_1 &= \left[a\cos\phi_0\cos\left(\frac{\Delta\alpha}{2}\right)\sin\left(\frac{\Delta\alpha}{2}\right)\right. \\ &\quad \left. - a\sin\phi_0\sin^2\left(\frac{\Delta\alpha}{2}\right)\right]N \end{aligned} \tag{A.7}$$

$$\begin{aligned} S_2 &= -\left[a\cos\phi_0\sin^2\left(\frac{\Delta\alpha}{2}\right)\right. \\ &\quad \left. + a\sin\phi_0\cos\left(\frac{\Delta\alpha}{2}\right)\sin\left(\frac{\Delta\alpha}{2}\right)\right]N. \end{aligned} \tag{A.8}$$

Squaring and adding yields

$$\mathrm{ac} = Na\sin\left(\frac{\Delta\alpha}{2}\right). \tag{A.9}$$

Substituting $\Delta\alpha$ as $\frac{2\pi}{N}$ as defined and normalizing to the limiting value as $N \to \infty$ (π) we obtain

$$\mathrm{ac} = \frac{Na}{\pi}\sin\left(\frac{\pi}{N}\right). \tag{A.10}$$

References

[1] Opsal J, Taylor M, Smith W and Rosencwaig A 1987 Temporal behaviour of modulated optical reflectance in silicon *J. Appl. Phys.* **61** 240–8

[2] Loriette V and Boccara C 2003 Absorption of low-loss optical materials measured at 1064 nm by a position modulated collinear photothermal detection technique *Appl. Opt.* **42** 649–56

[3] Murray T and Balogun O 2004 High-sensitivity laser-based acoustic microscopy using a modulated excitation source *Appl. Phys. Lett.* **85** 2974–6

[4] Thomsen C, Grahn H, Maris H and Tauc J 1986 Surface generation and diction of phonons by picosecond light pulses *Phys. Rev.* B **34** 4129–38

[5] Kuo P, Feng Z, Ahmed T, Favro L, Thomas R and Hartikainen J 1987 Parallel thermal wave imaging using a vector lock-in video technique *Photoacoustic and Photothermal Phenomena* ed H P Hess and J Pelzl (Heidelberg: Springer) pp 415–8

[6] Pitter M, See C and Somekh M 2004 Full-field heterodyne interference microscope with spatially incoherent illumination *Opt. Lett.* **29** 1200–2

[7] Thomsen C, Grahn H, Maris H and Tauc J 1986 Picosecond interferometric technique for study of phonons in the Brillouin frequency range *Opt. Commun.* **60** 55–8

[8] Grievenkamp J 1984 Generalized data reduction for heterodyne interferometry *Opt. Eng.* **23** 350–2

[9] Hooper I, Sambles J, Pitter M and Somekh M 2006 Phase sensitive array detection with polarisation modulated differential sensing *Sensors Actuators* B **119** 651–5

[10] Bourquin S, Prasankumar R, Kartner F, Fujimoto J, Lasser T and Salathe R 2003 High-speed femtosecond pump–probe spectroscopy with a smart pixel detector array *Opt. Lett.* **28** 1588–90

[11] Seitz P, Oggier T and Blanc N 2004 All solid-state optical time-of-flight 3D range imaging *Tech. Mess.* **71** 538–44

[12] Bourquin S, Seitz P and Salathé R 2001 Two-dimensional smart detector array for interferometric applications *Electron. Lett.* **37** 975–6

[13] Rossignol C, Rampnoux J, Dehoux T, Dilhaire S and Audoin B 2006 Picosecond ultrasonics time resolved spectroscopy using a photonic crystal fiber *Rev. Sci. Instrum.* **77** 033101

[14] Adachi S 1993 *Properties of Aluminium Gallium Arsenide* ed S Adachi (London, UK: INSPEC) pp 22–3